A coupling strategy for nonlocal and local diffusion models with mixed volume constraints and boundary conditions [1]

Marta D'Elia, Mauro Perego, Pavel Bochev, David Littlewood

Center for Computing Research
Sandia National Laboratories, Mail Stop 1320
Albuquerque, New Mexico, 87185-1320

Abstract

We develop and analyze an optimization–based method for the coupling of nonlocal and local diffusion problems with mixed volume constraints and boundary conditions. The approach formulates the coupling as a control problem where the states are the solutions of the nonlocal and local equations, the objective is to minimize their mismatch on the overlap of the nonlocal and local domains, and the controls are virtual volume constraints and boundary conditions. We prove that the resulting optimization problem is well–posed and discuss its implementation using Sandia's agile software components toolkit. The latter provides the groundwork for the development of engineering analysis tools, while numerical results for nonlocal diffusion in three–dimensions illustrate key properties of the optimization–based coupling method.

Keywords: Nonlocal models, coupling method, optimization, nonlocal vector calculus, mixed boundary conditions, nonlocal diffusion.

[1]Sandia National Laboratories is a multi-program laboratory managed and operated by Sandia Corporation, a wholly owned subsidiary of Lockheed Martin Corporation, for the U.S. Department of Energy's National Nuclear Security Administration under contract DE-AC04-94AL85000

1. Introduction

The use of nonlocal models in science and engineering applications has been steadily increasing over the past decade. The ability of nonlocal theories to accurately capture effects that are difficult or impossible to represent by local Partial Differential Equation (PDE) models motivates and drives the interest in this type of simulations.

For instance, potential–based atomistics provides an accurate representation of material defects, such as dislocations and interacting point defects, which play roles in determining the elastic and plastic response of a material [27]. Likewise, nonlocal continuum theories such as peridynamics [32, 34] or physics–based nonlocal elasticity [11] allow interactions at distance without contact and can accurately resolve small scale features such as crack tips and dislocations. Such models can also arise from homogenization of nonlinear damage models [15]. Similarly, nonlocal electrostatic models [17] have proved essential in, e.g., simulations of electrokinetic nanofluidic channels, where local response modification to Poisson–Boltzmann are qualitatively incorrect [4].

However, the improved accuracy of nonlocal models comes at the price of a significant increase in computational costs compared to, e.g., traditional PDEs. In particular, a complete nonlocal simulation remains computationally untenable for many science and engineering applications. Further, nonlocal models generally require the application of volume constraints, which are more difficult to specify in practice than the boundary conditions of the local theory. As a result, many researches have focused attention on the development of various Local–to–Nonlocal (LtN) coupling strategies, which aim to combine the accuracy of nonlocal models with the computational efficiency of PDEs. The basic idea is to use the more efficient PDE model everywhere except in those parts of the domain that require the improved accuracy of the nonlocal model.

Atomistic–to–Continuum coupling methods [22, 21] are perhaps the earliest and most established class of LtN formulations, dating back to the quasicontinuum approach [35]. Formulation of LtN couplings for material models such as peridynamics and continuum mechanics [15, 31, 20, 2] is a more recent development and is among the applications targeted by the coupling approach we develop in this paper.

Despite the differences in the type of models being coupled and the specific details of their coupling, the bulk of the existing LtN methods can be

described as variations of a "blending" approach. Blending methods merge models by using partition of unity, or a similar mechanism, to create a hybrid state on the overlap of the subdomains where the models operate. For instance, a typical energy–based AtC method defines a hybrid energy functional by mixing atomistic and continuum energies over a bridging domain [3, 22], whereas a force–based AtC method first derives the atomistic and continuum force balance equations and then blends them into a hybrid force balance equation.

In the context of nonlocal and local continuum models the extension of the Arlequin method [10, 15] and the morphing approach [20, 2] are analogues to energy–based AtC, whereas force–based coupling of peridynamics and continuum mechanics [31] is similar to force–based AtC. The LtN couplings mentioned above are examples of heterogeneous domain decomposition in which different mathematical models operating in different parts of the domain are coupled by imposing physically–motivated coupling conditions as constraints on blended energy or force balance equations.

The LtN coupling method in this paper differs fundamentally from these approaches because it reverses the roles of the coupling conditions and the models. Specifically, it couches the merging of the local and nonlocal models into a constrained optimization problem in which the models define the constraints, the coupling conditions provide the optimization objective, and suitable boundary and/or force data act as virtual controls. This divide and conquer strategy allows the models to operate independently from each other by exchanging information through the virtual controls.

Following this approach, we obtain a coupling method that does not exhibit spurious forces on the interface and by construction can recover any solution that is representable exactly by the discretizations of the models, i.e., it passes a "patch test" of an arbitrary order. Furthermore, solving independently the local and nonlocal problems enables us to use discretization methods and software tools optimized for each individual model. In particular, it allows us to implement the coupling by using Sandia's *Albany* [29] and *Peridigm* [26] codes for the local and nonlocal models, respectively, resulting in an efficient, three–dimensional simulation capability that can be applied to realistic problems.

This work continues our previous efforts to use optimization and control ideas for the development of LtN coupling methods. These efforts include both coupling of atomistic and continuum models [23, 24] as well as local and nonlocal diffusion equations [8, 7] with homogeneous Dirichlet volume con-

straints. The latter provide a simple, yet representative LtN setting, which we continue to study in this paper. Specifically, we focus on extending the formulation and analysis in [8, 7] to the case of nonlocal diffusion problems with mixed volume constraints.

Practical applications, such as a clamped bar, or a body with an insulated wall, which require specification of both states (displacements, temperatures and etc.) and "fluxes" (surface traction force, heat flux and etc.) on the boundaries and interaction regions, motivate our interest in this setting. Although the imposition of mixed volume constraints does not substantially change the core optimization–based formulation, it does introduce theoretical challenges that are not present in the case of a single Dirichlet volume constraint, studied in [7].

The paper is organized as follows. In Section 2 we review the basic concepts of the nonlocal vector calculus, a theory developed in [13] that allows us to study nonlocal problems in a way similar to how we study PDEs. Here, we also introduce the nonlocal and local mathematical problems. In Section 3 we formulate the LtN coupling method and prove its well–posedness by exploiting the nonlocal vector calculus and some of the theoretical results in [7]. In Section 4 we introduce a finite–dimensional approximation and present the results of three–dimensional numerical simulations employing a meshless discretization of a nonlocal model and a finite element discretization of a local model.

2. Preliminaries

Let Ω be a bounded open domain in $\mathbb{R}^d$, $d = 2, 3$, with Lipschitz–continuous boundary $\partial\Omega$. We introduce the nonlocal operators that describe the nonlocal mathematical model. Let $\boldsymbol{\alpha}(\boldsymbol{x}, \boldsymbol{y})\colon \mathbb{R}^d \times \mathbb{R}^d \to \mathbb{R}^d$ be an antisymmetric function, i.e. $\boldsymbol{\alpha}(\boldsymbol{y}, \boldsymbol{x}) = -\boldsymbol{\alpha}(\boldsymbol{x}, \boldsymbol{y})$. For the functions $u(\boldsymbol{x})\colon \mathbb{R}^d \to \mathbb{R}$ and $\boldsymbol{\nu}(\boldsymbol{x}, \boldsymbol{y})\colon \mathbb{R}^d \times \mathbb{R}^d \to \mathbb{R}^d$ we define the nonlocal *divergence* $\mathcal{D}\colon \mathbb{R}^d \to \mathbb{R}$ of $\boldsymbol{\nu}(\boldsymbol{x}, \boldsymbol{y})$ as

$$\mathcal{D}(\boldsymbol{\nu})(\boldsymbol{x}) := \int_{\mathbb{R}^d} (\boldsymbol{\nu}(\boldsymbol{x}, \boldsymbol{y}) + \boldsymbol{\nu}(\boldsymbol{y}, \boldsymbol{x})) \cdot \boldsymbol{\alpha}(\boldsymbol{x}, \boldsymbol{y})\, d\boldsymbol{y} \qquad \boldsymbol{x} \in \mathbb{R}^d \tag{1}$$

and the nonlocal *gradient* $\mathcal{G}\colon \mathbb{R}^d \times \mathbb{R}^d \to \mathbb{R}^d$ of $u(\boldsymbol{x})$ as

$$\mathcal{G}(u)(\boldsymbol{x}, \boldsymbol{y}) := (u(\boldsymbol{y}) - u(\boldsymbol{x}))\boldsymbol{\alpha}(\boldsymbol{x}, \boldsymbol{y}) \qquad \boldsymbol{x}, \boldsymbol{y} \in \mathbb{R}^d. \tag{2}$$

It is shown in [13] that the adjoint $\mathcal{D}^* = -\mathcal{G}$. Next, given a second–order symmetric positive semi–definite tensor $\boldsymbol{\Phi}(\boldsymbol{x},\boldsymbol{y}) = \boldsymbol{\Phi}(\boldsymbol{y},\boldsymbol{x})$ we define the nonlocal *diffusion* $\mathcal{L}\colon \mathbb{R}^d \to \mathbb{R}$ of $u(\boldsymbol{x})$ as a composition of the nonlocal divergence and gradient operators, i.e.

$$\mathcal{L}u(\boldsymbol{x}) := \mathcal{D}(\boldsymbol{\Phi}\mathcal{G}u)(\boldsymbol{x}) = 2\int_{\mathbb{R}^d} (u(\boldsymbol{y}) - u(\boldsymbol{x}))\,\gamma(\boldsymbol{x},\boldsymbol{y})\,d\boldsymbol{y} \qquad \boldsymbol{x}\in\mathbb{R}^d, \tag{3}$$

where $\gamma(\boldsymbol{x},\boldsymbol{y}) := \boldsymbol{\alpha}(\boldsymbol{x},\boldsymbol{y})\cdot\boldsymbol{\Phi}(\boldsymbol{x},\boldsymbol{y})\boldsymbol{\alpha}(\boldsymbol{x},\boldsymbol{y})$ is a non–negative symmetric kernel[2].

We define the *interaction domain* of an open bounded region $\Omega\in\mathbb{R}^d$ as

$$\widetilde{\Omega} = \{\boldsymbol{y}\in\mathbb{R}^d\setminus\Omega:\ \gamma(\boldsymbol{x},\boldsymbol{y})\neq 0,\ \boldsymbol{x}\in\Omega\},$$

and set $\Omega^+ = \Omega\cup\widetilde{\Omega}$. Note that, in general, $\widetilde{\Omega}$, and by extension Ω^+, may be unbounded even if Ω is bounded. To avoid unnecessary technical complications in this work we consider localized kernels γ such that for $\boldsymbol{x}\in\Omega$

$$\begin{cases} \gamma(\boldsymbol{x},\boldsymbol{y}) > 0 & \forall\,\boldsymbol{y}\in B_\varepsilon(\boldsymbol{x}) \\ \gamma(\boldsymbol{x},\boldsymbol{y}) = 0 & \forall\,\boldsymbol{y}\in\Omega^+\setminus B_\varepsilon(\boldsymbol{x}), \end{cases} \tag{4}$$

where $B_\varepsilon(\boldsymbol{x}) = \{\boldsymbol{y}\in\Omega^+:\ \|\boldsymbol{x}-\boldsymbol{y}\|<\varepsilon,\ \boldsymbol{x}\in\Omega\}$ and ε is the *interaction radius*. For such kernels the interaction domain is a layer of thickness ε that surrounds Ω, i.e.

$$\widetilde{\Omega} = \{\boldsymbol{y}\in\mathbb{R}^d\setminus\Omega:\ \|\boldsymbol{y}-\boldsymbol{x}\|<\varepsilon,\ \boldsymbol{x}\in\Omega\}. \tag{5}$$

We refer to Figure 1 (left) for an illustration of a two–dimensional region and its interaction domain.

Corresponding to the divergence operator $\mathcal{D}(\boldsymbol{\nu})$ we introduce a nonlocal *interaction* operator

$$\mathcal{N}(\boldsymbol{\nu})(\boldsymbol{x}) = -\int_{\Omega^+} (\boldsymbol{\nu}(\boldsymbol{x},\boldsymbol{y}) + \boldsymbol{\nu}(\boldsymbol{y},\boldsymbol{x}))\,\boldsymbol{\alpha}(\boldsymbol{x},\boldsymbol{y})\,d\boldsymbol{y} \qquad \boldsymbol{x}\in\widetilde{\Omega}. \tag{6}$$

[2]There are more general representations of the nonlocal diffusion operator, these are associated with non–symmetric and not necessarily positive kernel functions. In such cases $\mathcal{L}$ may define a model for non–symmetric diffusion phenomena, we mention e.g. non–symmetric jump processes [9].

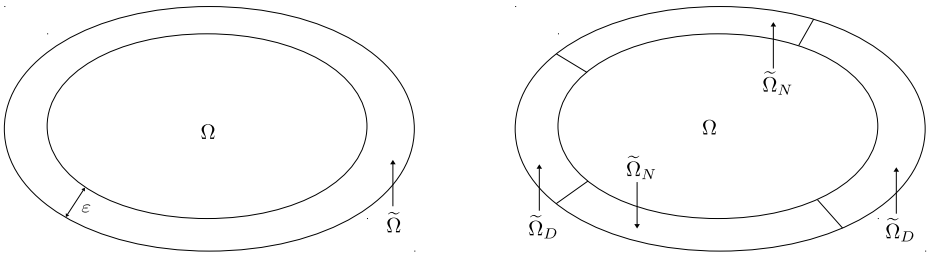

Figure 1: Left: two–dimensional domain Ω and interaction domain $\widetilde{\Omega}$. Right: for problem (9), two–dimensional domain Ω, Dirichlet interaction domain $\widetilde{\Omega}_D$ and Neumann interaction domain $\widetilde{\Omega}_N$.

The integral $\int_{\widetilde{\Omega}} \mathcal{N}(\boldsymbol{\nu})\, d\boldsymbol{x}$ generalizes the notion of a flux $\int_{\partial\Omega} \mathbf{q}\cdot\mathbf{n}\, dA$ through the boundary of a domain, with $\mathcal{N}(\boldsymbol{\nu})$ playing the role of a flux density $\mathbf{q}\cdot\mathbf{n}$. Of course the key difference between (6) and a conventional flux is that in the former the flux is a *volume* integral, whereas in the latter it is a *boundary* integral. Nonetheless, the nonlocal divergence and interaction operators satisfy a nonlocal Gauss theorem $\int_\Omega \mathcal{D}(\boldsymbol{\nu})\, d\boldsymbol{x} = \int_{\widetilde{\Omega}} \mathcal{N}(\boldsymbol{\nu})\, d\boldsymbol{x}$. We refer to [13] for additional nonlocal vector calculus results, including generalized nonlocal Green's identities. We respectively introduce the nonlocal energy semi–norm, nonlocal energy space, and nonlocal volume–constrained energy space

$$
\begin{aligned}
|||v|||^2_{\Omega^+} &:= \frac{1}{2}\int_{\Omega^+}\int_{\Omega^+} \mathcal{G}v\cdot(\boldsymbol{\Phi}\mathcal{G}v)\, d\boldsymbol{y}\, d\boldsymbol{x} \\
V(\Omega^+) &:= \{v\in L^2(\Omega^+)\ :\ |||v|||_{\Omega^+}<\infty\} \\
V_{\breve{\Omega}}(\Omega^+) &:= \left\{v\in V(\Omega^+)\ :\ v=0 \text{ on } \breve{\Omega}\right\} \quad \text{for } \breve{\Omega}\subseteq\widetilde{\Omega}.
\end{aligned}
\tag{7}
$$

For certain kernel functions the energy space is equivalent to standard spaces such as $L^2(\Omega^+)$ and the fractional Sobolev space $H^s(\Omega^+)$, $s\in(0,1)$; see [12]. We assume that for all $\breve{\Omega}\subseteq\widetilde{\Omega}$ with nonzero measure the energy norm satisfies a Poincaré–like inequality, i.e. $\|v\|_{0,\Omega^+}\le C_{pn}|||v|||_{\Omega^+}$ for all $v\in V_{\breve{\Omega}}(\Omega^+)$, where C_{pn} is referred to as the nonlocal Poincaré constant and $\|\cdot\|_{0,\Omega^+}$ is the L^2 norm over Ω^+. This property holds for a large class of kernel functions, see, e.g., cases 1 and 2 in [12, §4.2]. We also define the volume–trace space $\widetilde{V}(\breve{\Omega}) := \{v|_{\breve{\Omega}} : v\in V(\Omega^+)\}$, for $\breve{\Omega}\subseteq\widetilde{\Omega}$, and an associated norm

$$
\|\sigma\|_{\widetilde{V}(\breve{\Omega})} := \inf_{v\in V(\Omega^+), v|_{\breve{\Omega}}=\sigma} |||v|||_{\Omega^+}. \tag{8}
$$

2.1. Local–to–Nonlocal coupling setting

Let $\Omega \subset \mathbb{R}^d$ be a bounded open region with interaction domain $\widetilde{\Omega} \subset \mathbb{R}^d$. We assume that the nonlocal diffusion operator $\mathcal{L}$, with $\mathbf{\Phi} = \mathbf{I}$ chosen for simplicity, provides an accurate description of the physical processes of interest in $\Omega^+ = \Omega \cup \widetilde{\Omega}$.

In this paper we focus on the formulation and analysis of LtN methods for $\mathcal{L}$ augmented with mixed volume constraints. To this end we assume that the interaction domain is a union of two nonintersecting subdomains $\widetilde{\Omega}_D$ and $\widetilde{\Omega}_N$, respectively, i.e, $\widetilde{\Omega} = \widetilde{\Omega}_D \cup \widetilde{\Omega}_N$ and $\widetilde{\Omega}_D \cap \widetilde{\Omega}_N = \emptyset$; see Figure 1 (right). Then we consider the following volume–constrained nonlocal diffusion equation

$$\left\{ \begin{array}{rcll} -\mathcal{L}u_n & = & f_n & \boldsymbol{x} \in \Omega \\ u_n & = & \sigma_n & \boldsymbol{x} \in \widetilde{\Omega}_D \\ -\mathcal{N}(\mathcal{G}u_n) & = & \eta_n & \boldsymbol{x} \in \widetilde{\Omega}_N, \end{array} \right. \tag{9}$$

where $f_n \in L^2(\Omega)$, $\sigma_n \in \widetilde{V}(\widetilde{\Omega}_D)$ and $\eta_n \in L^2(\widetilde{\Omega}_N)$.

Volume constraints, i.e., constraints acting on domains having nonzero volume, are the nonlocal counterparts of boundary conditions for PDEs. In particular, the volume constraints on $\widetilde{\Omega}_D$ and $\widetilde{\Omega}_N$ are the nonlocal analogues of a Dirichlet boundary condition and a Neumann boundary condition, respectively. Multiplication of (9) by a test function $z_n \in V_{\widetilde{\Omega}_D}(\Omega^+)$, integration over Ω and application of the first nonlocal Green's identity [13] yield the following weak form of the nonlocal problem:

$$\int_{\Omega^+}\int_{\Omega^+} \mathcal{G}u_n \cdot \mathcal{G}z_n \, d\boldsymbol{y} \, d\boldsymbol{x} = \int_{\widetilde{\Omega}_N} \eta_n \, z_n \, d\boldsymbol{x} + \int_{\Omega} f_n z_n \, d\boldsymbol{x} \quad \forall z_n \in V_{\widetilde{\Omega}_D}(\Omega^+). \tag{10}$$

The weak form (10) confirms that the Neumann volume constraint plays a role similar to that of a conventional Neumann boundary condition by providing a forcing term acting on the interaction domain. We make the additional assumption that (9) is well–posed, i.e., (10) has a unique solution such that[3]

$$|||u_n|||_{\Omega^+} \leq K_n(\|f_n\|_{0,\Omega} + \|\sigma_n\|_{\widetilde{V}(\widetilde{\Omega}_D)} + \|\eta_n\|_{0,\widetilde{\Omega}_N}) \tag{11}$$

for some positive constant K_n.

[3]One can show that (10) is well–posed for a positive definite $\mathbf{\Phi}$ [13].

The nonlocal problem (9) can be discretized by a number of different methods either directly or by using its weak form (10); see, e.g., [6, 1, 5, 28, 25, 18] and the references therein. However, as the extent of the nonlocal interactions necessary to capture long range forces increases, so does the bandwidth of the algebraic systems resulting from any discretization of (9). This makes the numerical solution of (9) in all of Ω^+ expensive or not even feasible.

As an example, in the case of finite element discretizations, depending on the relationship between the mesh size and the interaction radius ε the bandwidth of the finite element matrix can be significantly larger than that for the local problem [8].

The key idea of an LtN simulation strategy is to improve the computational efficiency by using (9) only where strong nonlocal effects must be properly accounted for and switch to a more efficient local model elsewhere. A fundamental prerequisite for employing such a strategy is the availability of a local model that can accurately approximate all sufficiently "nice" solutions of (9). In the present context, such a model is provided by the local diffusion model given by the Poisson equation

$$\left\{\begin{array}{rcll} -\Delta u_l & = & f_l & \boldsymbol{x} \in \Omega^+ \\ u_l & = & \sigma_l & \boldsymbol{x} \in \Gamma_D \\ \nabla u_l \cdot \mathbf{n} & = & \eta_l & \boldsymbol{x} \in \Gamma_N, \end{array}\right. \tag{12}$$

where $\Gamma_D = \partial\Omega^+ \cap \widetilde{\Omega}_D$ and $\Gamma_N = \partial\Omega^+ \cap \widetilde{\Omega}_N$, and $f_l \in L^2(\Omega^+)$, $\sigma_l \in H^{\frac{1}{2}}(\Gamma_D)$ and $\eta_l \in L^2(\Gamma_N)$ are suitable forcing term and boundary data, respectively. Assumptions on $\widetilde{\Omega}_D$ and $\widetilde{\Omega}_N$ imply that $\Gamma_D \cap \Gamma_N = \emptyset$ and $\Gamma_D \cup \Gamma_N = \partial\Omega^+$. We refer to [13] for results showing that (12) is a good approximation of (9), whenever the latter has sufficiently regular solutions.

3. Optimization–based LtN formulation

Without loss of generality we consider (9) and (12) with homogeneous Dirichlet constraints on $\widetilde{\Omega}_D$ and Γ_D and homogeneous Neumann constraints on $\widetilde{\Omega}_N$ and Γ_N. We assume that these problems act on two overlapping subdomains of Ω^+. Thus we introduce a partition of Ω^+ into a nonlocal subdomain Ω_n with interaction volume $\widetilde{\Omega}_n$ and a local subdomain Ω_l, such that $\Omega_n^+ := \Omega_n \cup \widetilde{\Omega}_n \subset \Omega^+$ and $\Omega_b = \Omega_n^+ \cap \Omega_l \neq \emptyset$; see Figure 2 for a two–dimensional example. The key assumption in LtN couplings is that

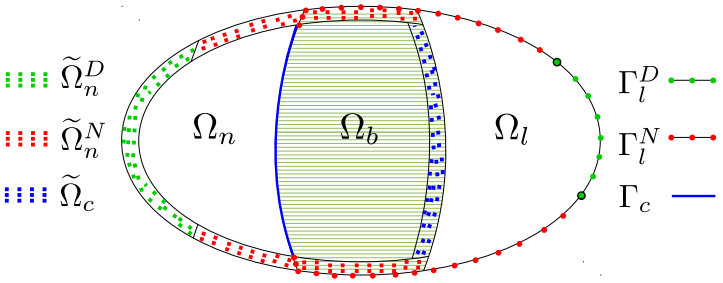

Figure 2: Two–dimensional coupling configuration.

accurate description of the material behavior in Ω_n requires the nonlocal model (9), whereas (12) provides a fair representation for the rest of the domain. Our coupling strategy consists in minimizing the difference between local and nonlocal solutions in the overlap region Ω_b tuning their values on the "virtual" interaction volumes and boundaries induced by the partition.

To this end we set

$$\widetilde{\Omega}_n^D = \widetilde{\Omega}_n \cap \widetilde{\Omega}_D, \quad \widetilde{\Omega}_n^N = \widetilde{\Omega}_n \cap \widetilde{\Omega}_N, \quad \text{and} \quad \widetilde{\Omega}_c = \widetilde{\Omega}_n \setminus (\widetilde{\Omega}_n^D \cup \widetilde{\Omega}_n^N),$$

so that $\widetilde{\Omega}_n = \widetilde{\Omega}_n^D \cup \widetilde{\Omega}_n^N \cup \widetilde{\Omega}_c$. Likewise, we set

$$\Gamma_l^D = \partial\Omega_l \cap \Gamma_D, \quad \Gamma_l^N = \partial\Omega_l \cap \Gamma_N, \quad \text{and} \quad \Gamma_c = \partial\Omega_l \setminus (\Gamma_l^D \cup \Gamma_l^N),$$

so that $\partial\Omega_l = \Gamma_l^D \cup \Gamma_l^N \cup \Gamma_c$; see Figure 2. Specification of a volume constraint on $\widetilde{\Omega}_c$ and a Dirichlet condition on Γ_c allows one to adjust the subdomain solutions. The restrictions of (9) and (12) to the nonlocal and local subdomains yield

$$\left\{\begin{array}{rcll} -\mathcal{L}u_n &=& f_n & \boldsymbol{x} \in \Omega_n \\ u_n &=& \theta_n & \boldsymbol{x} \in \widetilde{\Omega}_c \\ u_n &=& 0 & \boldsymbol{x} \in \widetilde{\Omega}_n^D \\ -\mathcal{N}(\mathcal{G}u_n) &=& 0 & \boldsymbol{x} \in \widetilde{\Omega}_n^N \end{array}\right. \quad \text{and} \quad \left\{\begin{array}{rcll} -\Delta u_l &=& f_l & \boldsymbol{x} \in \Omega_l \\ u_l &=& \theta_l & \boldsymbol{x} \in \Gamma_c \\ u_l &=& 0 & \boldsymbol{x} \in \Gamma_l^D \\ \nabla u_l \cdot \mathbf{n} &=& 0 & \boldsymbol{x} \in \Gamma_l^N, \end{array}\right. \tag{13}$$

where $\theta_n \in \Theta_n = \{v_n|_{\widetilde{\Omega}_c} : v_n \in V_{\widetilde{\Omega}_n^D}(\Omega_n^+)\}$ and $\theta_l \in H^{\frac{1}{2}}(\Gamma_c)$ are an undetermined volume constraint and a Dirichlet boundary condition, respectively. As we show later, the parameter space $\Theta_n \times \Theta_l$ is Hilbert with respect to the L^2 and $H^{\frac{1}{2}}$ metrics.

In this paper we study an optimization–based LtN coupling comprising the following constrained optimization problem

$$\min_{u_n,u_l,\theta_n,\theta_l} J(u_n,u_l)=\frac{1}{2}\int_{\Omega_b}(u_n-u_l)^2\,d\boldsymbol{x}=\frac{1}{2}\|u_n-u_l\|^2_{0,\Omega_b}\quad\text{subject to (13).}\tag{14}$$

In the terminology of optimization and control problems, the subdomain problems (13) are the optimization constraints, u_n and u_l are the states, and θ_n and θ_l are the controls.

The absence of control penalty terms $\beta_n\|\theta_n\|^2_{0,\widetilde{\Omega}_c}$ and $\beta_l\|\theta_l\|^2_{1/2,\Gamma_c}$ in the objective is a notable feature of the optimization formulation (14). Typically, such terms are required to ensure the well–posedness of the optimization problem; however, the analysis in the following section reveals that the control penalty is not necessary for the well–posedness of (14).

Another notable feature of (14), which distinguishes it from conventional LtN approaches, is the absence of any blending between the nonlocal and local subproblems over Ω_b. Instead, as constraints, these problems act independently on Ω_n^+ and Ω_l and communicate implicitly through the virtual controls.

Following [7] we define the LtN solution $u^*\in L^2(\Omega^+)$ as

$$u^*=\begin{cases} u_n^* & \boldsymbol{x}\in\Omega_n^+\\ u_l^* & \boldsymbol{x}\in\Omega_l\setminus\Omega_b,\end{cases}\tag{15}$$

where $(u_n^*,u_l^*,\theta_n^*,\theta_l^*)\in V_{\widetilde{\Omega}_n^D}(\Omega_n^+)\times H^1_{\Gamma_l^D}(\Omega_l)\times\Theta_n\times\Theta_l$ is an optimal solution of (14). In the next section we prove the well–posedness of (14), i.e. the uniqueness of u^*.

3.1. Well–posedeness

We rewrite the optimization problem (14) in terms of the control variables only. Under the assumption of well–posedness of the constraints, for any pair (θ_n,θ_l) the subproblems in (13) have unique solutions $u_n(\theta_n)$ and $u_l(\theta_l)$. Substitution of these states into the functional yields the so called reduced space form of (14)

$$\min_{\theta_n,\theta_l} J(\theta_n,\theta_l)=\frac{1}{2}\int_{\Omega_b}(u_n(\theta_n)-u_l(\theta_l))^2\,d\boldsymbol{x}=\frac{1}{2}\|u_n(\theta_n)-u_l(\theta_l)\|^2_{0,\Omega_b}.\tag{16}$$

Following [7] we split, for any given (θ_n, θ_l), the solutions of the state equations into a harmonic and a homogeneous part as follows

$$u_n(\theta_n) = v_n(\theta_n) + u_n^0 \qquad \text{and} \qquad u_l(\theta_l) = v_l(\theta_l) + u_l^0, \tag{17}$$

where the harmonic components $v_n(\theta_n)$ and $v_l(\theta_l)$ solve the equations

$$\left\{\begin{array}{rcl} -\mathcal{L}v_n &=0 & \boldsymbol{x}\in\Omega_n \\ v_n &=\theta_n & \boldsymbol{x}\in\widetilde{\Omega}_c \\ v_n &=0 & \boldsymbol{x}\in\widetilde{\Omega}_n^D \\ -\mathcal{N}(\mathcal{G}v_n) &=0 & \boldsymbol{x}\in\widetilde{\Omega}_n^N \end{array}\right. \quad \text{and} \quad \left\{\begin{array}{rcl} -\Delta v_l &=0 & \boldsymbol{x}\in\Omega_l \\ v_l &=\theta_l & \boldsymbol{x}\in\Gamma_c \\ v_l &=0 & \boldsymbol{x}\in\Gamma_l^D \\ \nabla v_l\cdot\mathbf{n} &=0 & \boldsymbol{x}\in\Gamma_l^N \end{array}\right. \tag{18}$$

respectively, whereas the homogeneous components u_n^0 and u_l^0 solve

$$\left\{\begin{array}{rcl} -\mathcal{L}u_n^0 &=f_n & \boldsymbol{x}\in\Omega_n \\ u_n^0 &=0 & \boldsymbol{x}\in\widetilde{\Omega}_n^D\cup\widetilde{\Omega}_c \\ -\mathcal{N}(\mathcal{G}u_n^0) &=0 & \boldsymbol{x}\in\widetilde{\Omega}_n^N \end{array}\right. \quad \text{and} \quad \left\{\begin{array}{rcl} -\Delta u_l^0 &=f_l & \boldsymbol{x}\in\Omega_l \\ u_l^0 &=0 & \boldsymbol{x}\in\Gamma_l^D\cup\Gamma_c \\ \nabla u_l^0\cdot\mathbf{n} &=0 & \boldsymbol{x}\in\Gamma_l^N \end{array}\right. \tag{19}$$

respectively. According to (17) $J(\theta_n, \theta_l)$ assumes the form

$$J(\theta_n,\theta_l) = \frac{1}{2}\|v_n(\theta_n)-v_l(\theta_l)\|^2_{0,\Omega_b} + (u_n^0-u_l^0, v_n(\theta_n)-v_l(\theta_l))_{0,\Omega_b} + \frac{1}{2}\|u_n^0-u_l^0\|^2_{0,\Omega_b}\,.$$

Setting the first variations of $J(\theta_n, \theta_l)$ with respect to θ_n and θ_l to zero and using that $v_n(\theta_n)$ and $v_l(\theta_l)$ are linear functions of the controls yields the following first–order optimality system (Euler–Lagrange equation) for (16): seek $(\sigma_n, \sigma_l) \in \Theta_n \times \Theta_l$ such that

$$Q(\sigma_n,\sigma_l;\mu_n,\mu_l) = F(\mu_n,\mu_l) \quad \forall(\mu_n,\mu_l)\in\Theta_n\times\Theta_l, \tag{20}$$

where $F(\mu_n, \mu_l) = -(u_n^0 - u_l^0, v_n(\mu_n) - v_l(\mu_l))_{0,\Omega_b}$ is an affine functional and

$$Q(\sigma_n,\sigma_l;\mu_n,\mu_l) = (v_n(\sigma_n) - v_l(\sigma_l),\, v_n(\mu_n) - v_l(\mu_l))_{0,\Omega_b}$$

is a symmetric bilinear form.

We show that (16) is well–posed by proving that $Q(\cdot;\cdot)$ defines an inner product. The proof relies on the fact that the solutions of (18) satisfy maximum principles. The following lemma reviews the maximum principle that holds for the solution of the local harmonic problem.

Lemma 3.1. *For the local problem in (18) we have (see e.g. [30])*

$$\sup_{\Omega_l} v_l \leq \sup_{\Gamma_c \cup \Gamma_l^D} v_l, \quad \textit{and} \quad \inf_{\Omega_l} v_l \geq \inf_{\Gamma_c \cup \Gamma_l^D} v_l. \tag{21}$$

A similar result holds for the solution of the nonlocal problem in (18).

Lemma 3.2. *For the nonlocal problem in (18) we have*

$$\sup_{\widetilde{\Omega}_n^N \cup \Omega_n} v_n \leq \sup_{\widetilde{\Omega}_c \cup \widetilde{\Omega}_n^D} v_n; \tag{22}$$

in particular, if $\sup_{\widetilde{\Omega}_n^N \cup \Omega_n} v_n = \sup_{\widetilde{\Omega}_c \cup \widetilde{\Omega}_n^D} v_n$*, then* v_n *is constant. Also,*

$$\inf_{\widetilde{\Omega}_n^N \cup \Omega_n} v_n \geq \inf_{\widetilde{\Omega}_c \cup \widetilde{\Omega}_n^D} v_n$$

and if $\inf_{\widetilde{\Omega}_n^N \cup \Omega_n} v_n = \inf_{\widetilde{\Omega}_c \cup \widetilde{\Omega}_n^D} v_n$*, then* v_n *is constant.*

Proof. We show that if $\sup_{\Omega_n^+} v_n = \sup_{\widetilde{\Omega}_n^N \cup \Omega_n} v_n$ then v_n is constant, which also implies that (22) holds. The results related to the infimum can be proved analogously. Let $K = \sup_{\Omega_n^+} v_n$. There exists $\overline{\boldsymbol{x}} \in \widetilde{\Omega}_n^N \cup \Omega_n$ such that

$$\sup_{\Sigma_{\frac{1}{3}}(\overline{\boldsymbol{x}})} v_n = K, \quad \text{with } \Sigma_q(\overline{\boldsymbol{x}}) := B_{q\,\varepsilon}(\overline{\boldsymbol{x}}) \cap (\widetilde{\Omega}_n^N \cup \Omega_n).$$

Assume that v_n is non–constant in $\Sigma_{\frac{2}{3}}(\overline{\boldsymbol{x}})$, i.e. for some $\delta > 0$ there exists a set of nonzero measure $S(\overline{\boldsymbol{x}}) \subset \Sigma_{\frac{2}{3}}(\overline{\boldsymbol{x}})$ where $v_n \leq K - \delta$. Because of the properties of the supremum, for any $k = 1, 2, \ldots$ there exists a set of nonzero measure $S_k \in \Sigma_{\frac{1}{3}}(\overline{\boldsymbol{x}})$ such that for any $\boldsymbol{x}_k \in S_k$, $v_n(\boldsymbol{x}_k) \geq K - \frac{1}{k}$. Using these bounds together with the kernel locality assumption (4), the nonlocal Neumann constraint $\mathcal{N}(\mathcal{G}v_n) = 0$ in $\widetilde{\Omega}_n^N$, and the nonlocal equation $\mathcal{L}v_n = 0$

in Ω_n, we find that for any $\boldsymbol{x}_k \in S_k$

$$\begin{aligned} v_n(\boldsymbol{x}_k) &= \frac{\displaystyle\int_{B_\varepsilon(\boldsymbol{x}_k)\cap\Omega_n^+} v_n(\boldsymbol{y})\gamma(\boldsymbol{x}_k,\boldsymbol{y})\,d\boldsymbol{y}}{\displaystyle\int_{B_\varepsilon(\boldsymbol{x}_k)\cap\Omega_n^+} \gamma(\boldsymbol{x}_k,\boldsymbol{y})\,d\boldsymbol{y}} \\ &= \frac{\displaystyle\int_{B_\varepsilon(\boldsymbol{x}_k)\cap\Omega_n^+\setminus S(\overline{\boldsymbol{x}})} v_n(\boldsymbol{y})\gamma(\boldsymbol{x}_k,\boldsymbol{y})\,d\boldsymbol{y} + \int_{S(\overline{\boldsymbol{x}})} v_n(\boldsymbol{y})\gamma(\boldsymbol{x}_k,\boldsymbol{y})\,d\boldsymbol{y}}{\displaystyle\int_{B_\varepsilon(\boldsymbol{x}_k)\cap\Omega_n^+} \gamma(\boldsymbol{x}_k,\boldsymbol{y})\,d\boldsymbol{y}} \\ &\le \frac{\displaystyle K\int_{B_\varepsilon(\boldsymbol{x}_k)\cap\Omega_n^+} \gamma(\boldsymbol{x}_k,\boldsymbol{y})\,d\boldsymbol{y} - \delta\int_{S(\overline{\boldsymbol{x}})} \gamma(\boldsymbol{x}_k,\boldsymbol{y})\,d\boldsymbol{y}}{\displaystyle\int_{B_\varepsilon(\boldsymbol{x}_k)\cap\Omega_n^+} \gamma(\boldsymbol{x}_k,\boldsymbol{y})\,d\boldsymbol{y}} \\ &\le K - C_\delta \le v_n(\boldsymbol{x}_k) + \tfrac{1}{k} - C_\delta, \end{aligned}$$

where C_δ is a positive constant that does not depend on k. For a large enough k the inequality $v_n(\boldsymbol{x}_k) \le v_n(\boldsymbol{x}_k) + \frac{1}{k} - C_\delta$ leads to a contradiction. As a consequence, v_n must be constant in $\Sigma_{\frac{2}{3}}(\overline{\boldsymbol{x}})$. We can move to another point $\overline{\boldsymbol{x}}_1 \in \Sigma_{\frac{2}{3}}(\overline{\boldsymbol{x}}_1)$ and repeat the argument and conclude that v_n is constant in $\Sigma_{\frac{2}{3}}(\overline{\boldsymbol{x}}_1)$ until we cover all the domain. Notice that instead of $\Sigma_{\frac{1}{3}}$ and $\Sigma_{\frac{2}{3}}$ we can choose Σ_p and Σ_{1-p}, for any positive $p < 1$. In this way we can prove that v_n is constant in Ω_n^+. □

Lemma 3.3. *The form $Q(\cdot;\cdot)$ defines an inner product on $\Theta_n \times \Theta_l$.*

Proof. Since by construction the bilinear form $Q(\cdot,\cdot)$ is symmetric and positive semi–definite, we only need to prove its positive definiteness, i.e.,

$Q(\sigma_n,\sigma_l;\sigma_n,\sigma_l) = 0$ if and only if $(\sigma_n,\sigma_l) = (0,0)$.

Suppose $Q(\sigma_n,\sigma_l;\sigma_n,\sigma_l) = 0$, then $v_n(\sigma_n) - v_l(\sigma_l) = 0$ in Ω_b. Let $v = v_n(\sigma_n) = v_l(\sigma_l)$ in Ω_b, our goal is to show that $v = 0$ in Ω_b. We do this by contradiction, assuming v is nonzero. This implies that v is nonzero over $\widetilde{\Omega}_c$, otherwise, because of Lemma 3.2 it would be zero on Ω_b.

We assume, without loss of generality, that $v > 0$ on a set with nonzero measure contained in $\widetilde{\Omega}_c$. Then, we have

$$\sup_{\widetilde{\Omega}_c} v \le \sup_{\Gamma_c} v \le \sup_{\widetilde{\Omega}_c} v,$$

where the first inequality is a consequence of Lemma 3.1 and the second of Lemma 3.2. Therefore, we have that $\sup_{\widetilde{\Omega}_c} v = \sup_{\Gamma_c} v$ and hence, v must be constant. $\square$

The next two lemmas require the following assumptions on the kernel γ:

$$\overline{\gamma}_1 < \infty \quad \text{and} \quad \overline{\gamma}_2 < \infty, \quad \text{where} \tag{23}$$

$$\gamma_k(\boldsymbol{x}) = \int_{\Omega^+} \gamma^k(\boldsymbol{x}, \boldsymbol{y})\, d\boldsymbol{y}, \qquad \text{and} \qquad \overline{\gamma}_k = \|\gamma_k\|_\infty^{1/k}, \quad k = 1, 2. \tag{24}$$

In the remainder of the section C_i, $i = 1, 2, \ldots$, denote generic positive constants and $C(\Omega)$ denotes a positive constant that depends on $|\Omega|$.

Lemma 3.4. *The space $\widetilde{V}_{\breve{\Omega}}(\widehat{\Omega}) = \{\mu_n = w|_{\widehat{\Omega}} : w \in V_{\breve{\Omega}}(\Omega^+)\}$ is a closed subspace of $L^2(\widehat{\Omega})$ for any $\widehat{\Omega} \subset \widetilde{\Omega}$ and $\breve{\Omega} \subset \widetilde{\Omega}$. Thus, $\widetilde{V}_{\breve{\Omega}}(\widehat{\Omega})$ is Hilbert with respect to the L^2 inner product.*

Proof. Consider a sequence $\{\mu^k\} \subset \widetilde{V}_{\breve{\Omega}}(\widehat{\Omega})$ such that $\mu^k \to \mu^* \in L^2(\widehat{\Omega})$; next, consider the function $w^* \in L^2(\Omega^+)$ such that

$$w^*|_{\widehat{\Omega}} = \mu^* \quad \text{and} \quad w^*|_{\Omega^+ \setminus \widehat{\Omega}} = 0.$$

To complete the proof it remains to show that $w^* \in V_{\breve{\Omega}}(\Omega^+)$, i.e. that w^* has finite energy norm. Using the equivalence of the energy norm and the L^2 norm (see [7]) we have

$$|||w^*|||_{\Omega^+} \leq C(\Omega^+)\|w^*\|_{0,\Omega^+} = \|\mu^*\|_{0,\widehat{\Omega}} < \infty.$$

Therefore, $w^* \in V_{\breve{\Omega}}(\Omega^+)$ and $w^*|_{\widehat{\Omega}} = \mu^*$, hence $\mu^* \in \widetilde{V}_{\breve{\Omega}}(\widehat{\Omega})$. $\square$

Lemma 3.5. *The space $\Theta_n \times \Theta_l$ is Hilbert with respect to the inner product* $Q(\sigma_n, \sigma_l; \mu_n, \mu_l) = (v_n(\sigma_n) - v_l(\sigma_l),\, v_n(\mu_n) - v_l(\mu_l))_{0,\Omega_b}$.

Proof. As a consequence of Lemma 3.4, the space $\Theta_n \times \Theta_l$ is Hilbert with respect to the inner product of $L^2(\widetilde{\Omega}_c) \times H^{\frac{1}{2}}(\Gamma_c)$ and in Lemma 3.3 we showed that Q is an inner product. We have to show that $\Theta_n \times \Theta_l$ is complete with the norm induced by Q: $\|(\sigma_n, \sigma_l)\|_*^2$. We do this by showing that $\|(\sigma_n, \sigma_l)\|_*^2$ is equivalent to the norm $\|(\sigma_n, \sigma_l)\|_{\Theta_n \times \Theta_l}^2 = \|\sigma_n\|_{0,\widetilde{\Omega}_c}^2 + \|\sigma_l\|_{\frac{1}{2},\Gamma_c}^2$, i.e.

$$C_1\|(\sigma_n, \sigma_l)\|_{\Theta_n \times \Theta_l}^2 \leq \|(\sigma_n, \sigma_l)\|_*^2 \leq C_2\|(\sigma_n, \sigma_l)\|_{\Theta_n \times \Theta_l}^2.$$

By the well–posedness of both problems we have that for all $(\sigma_n, \sigma_l) \in \Theta_n \times \Theta_l$

$$\begin{aligned}
\|(\sigma_n, \sigma_l)\|_*^2 &= \|v_n(\sigma_n) - v_l(\sigma_l)\|_{0,\Omega_b}^2 \\
&\leq \|v_n(\sigma_n)\|_{0,\Omega_b}^2 + \|v_l(\sigma_l)\|_{0,\Omega_b}^2 \\
&\leq C_{pn}^2 |||v_n(\sigma_n)|||_{\Omega_n^+}^2 + \|v_l(\sigma_l)\|_{H^1(\Omega_l)}^2 \\
&\leq C_{pn}^2 K_n^2 \|\overline{\sigma}_n\|_{\widetilde{V}_{\widetilde{\Omega}_n^D}(\widetilde{\Omega}_n^D \cup \widetilde{\Omega}_c)}^2 + K_l^2 \|\sigma_l\|_{\frac{1}{2},\Gamma_c}^2,
\end{aligned}$$

where $\overline{\sigma}_n$ is an extension to 0 of σ_n in $\widetilde{\Omega}_n^D$ and K_l is the stability constant for the local problem in (18). Also, by a nonlocal trace theorem ([7], Lemma A.1) and by the equivalence of the energy and the L^2 norms ([7], Lemma A.2) we have

$$\begin{aligned}
\|(\sigma_n, \sigma_l)\|_*^2 &\leq C_3 |||\overline{\sigma}_n|||_{\widetilde{\Omega}_n^D \cup \widetilde{\Omega}_c}^2 + K_l^2 \|\sigma_l\|_{\frac{1}{2},\Gamma_c}^2 \\
&\leq C_4 \|\overline{\sigma}_n\|_{0,\widetilde{\Omega}_n^D \cup \widetilde{\Omega}_c}^2 + K_l^2 \|\sigma_l\|_{\frac{1}{2},\Gamma_c}^2 \\
&\leq C_5 \left(\|\sigma_n\|_{0,\widetilde{\Omega}_c}^2 + \|\sigma_l\|_{\frac{1}{2},\Gamma_c}^2 \right).
\end{aligned}$$

Next, by using Lemma A.4 in [7], we can show that

$$\|v_n(\sigma_n)\|_{0,\Omega_b}^2 + \|v_l(\sigma_l)\|_{0,\Omega_b}^2 \leq C(\Omega_b) \|v_n(\sigma_n) - v_l(\sigma_l)\|_{0,\Omega_b}^2.$$

Because $\widetilde{\Omega}_c \subset \Omega_b$ and $\sigma_n = v_n|_{\widetilde{\Omega}_c}$, we have $\|\sigma_n\|_{0,\widetilde{\Omega}_c}^2 \leq \|v_n\|_{0,\Omega_b}^2$. For the local problem, by combining the trace inequality [30] and the Caccioppoli inequality for harmonic functions, we obtain

$$\|\sigma_l\|_{H^{\frac{1}{2}}(\Gamma_c)}^2 \leq \|v_n\|_{H^1(\Omega_b)}^2 = \|v_n\|_{0,\Omega_b}^2 + |v_n|_{H^1(\Omega_b)}^2 \leq (1 + C(\Omega_b)) \|v_n\|_{0,\Omega_b}. \quad (25)$$

□

The following result is a direct consequence of Lemmas 3.3 and 3.5 and the projection theorem.

Theorem 3.1. *The reduced space problem (16) has a unique minimizer.*

4. Numerical solution of the optimization–based LtN formulation

This section presents a discretization of the optimization–based LtN formulation and outlines a gradient–based method for finding an approximate minimizer of the discrete problem.

As mentioned above, one of the most attractive features of our coupling method is the fact that the local and nonlocal problems can be solved independently, without any blending over Ω_b. This means that one can utilize two fundamentally different discretization methods. In this work, we employ a meshfree discretization for the nonlocal problem and a finite element discretization for the local problem, both of which are described in the following section.

4.1. Discretization schemes

We obtain the solution for the nonlocal diffusion problem by discretizing the strong form of (9) using a meshfree approach that follows Silling and Askari [33, 26, 19]. Under this procedure, the nonlocal domain is represented by a set of material points, each of which is assigned a (scalar) volume. The integral expression given by (3) is approximated as a summation,

$$\mathcal{L}u(\boldsymbol{x}) \approx 2\sum_{i=1}^{N_{\boldsymbol{x}}} \left(u(\boldsymbol{y}_i) - u(\boldsymbol{x})\right) \gamma(\boldsymbol{x}, \boldsymbol{y}_i)\, V_{\boldsymbol{y}_i}, \tag{26}$$

where the summation is taken over the $N_{\boldsymbol{x}}$ material points that are within a distance ε of material point $\boldsymbol{x}$, and $V_{\boldsymbol{y}_i}$ is the volume associated with material point $\boldsymbol{y}_i$.

For the approximation of the local problem we employ a finite element discretization of the weak form of (12). Let $V_{\theta_l} := \{v \in H^1_{\Gamma_l^D}(\Omega_l) : v|_{\Gamma_c} = \theta_l \in \Theta_l\}$. The weak solution $u_l(\theta_l) \in V_{\theta_l}$ solves the variational equation

$$\int_{\Omega_l} \nabla u_l \nabla z_l \, d\boldsymbol{x} = \int_{\Omega_l} f_l z_l \, d\boldsymbol{x}, \tag{27}$$

for all $z_l \in H^1_{\Gamma_l^D \cup \Gamma_c}$. We consider the finite–dimensional spaces

$$H^h_{\Gamma_l^D} \subset H^1_{\Gamma_l^D}(\Omega_l), \quad \Theta_l^h \subset \Theta_l, \quad V^h_{\theta_l^h} := \{v \in H^h_{\Gamma_l^D}(\Omega_l) : v|_{\Gamma_c} = \theta_l^h \in \Theta_l^h\}. \tag{28}$$

The parameter $h > 0$ describes the resolution of a discrete space and is proportional to the inverse of its dimension. We assume that the spaces in

(28) are such that the sequence of best approximations, to any function in the infinite–dimensional space, converges as $h \to 0$. The finite dimension approximation of (27) reads: Find $u_{lh} \in V^h_{\theta^h_l}$ such that

$$\int_{\Omega_l} \nabla u_{lh} \nabla z_{lh} \, d\boldsymbol{x} = \int_{\Omega_l} f_l z_{lh} \, d\boldsymbol{x}, \tag{29}$$

for all $z_{lh} \in H^h_{\Gamma^D_l \cup \Gamma_c}(\Omega_l) := \{v \in H^h_{\Gamma^D_l}(\Omega_l) : v|_{\Gamma_c} = 0\}$.

Because the meshfree discretization scheme utilized for the nonlocal model does not readily support the calculation of a continuous functional, it is convenient to instead consider a "discrete" functional in which the difference between the local and the nonlocal solutions is taken pointwise. For the example simulations presented below, the functional is evaluated at the locations of the material points of the nonlocal model within the overlap region Ω_b. The solution for the local model is interpolated to these locations using the finite–element shape functions employed in the discretization of the local problem. The objective function for the optimization routine is then defined as the ℓ_2-norm of the pointwise differences between the local and nonlocal solutions.

Let $\mathbf{u}_n \in \mathbb{R}^{N_n}$ be the vector of pointwise values of the nonlocal solution and $\mathbf{u}_l \in \mathbb{R}^{N_l}$ be the vector of values of the local solution corresponding to the finite element degrees of freedom. Also, let N_b be the number of degrees of freedom of $\mathbf{u}_n$ in Ω_b. We define the nonlocal selection matrix $S_n \in \mathbb{R}^{N_b, N_n}$ as the operator that selects the components of $\mathbf{u}_n$ in Ω_b[4]:

$$S_n = [\, O_{N_b, N_n - N_b} \quad I_{N_b} \,].$$

We define the local selection matrix $S_l \in \mathbb{R}^{N_b, N_l}$ as the operator that evaluates $\mathbf{u}_l$ on the degrees of freedom of $\mathbf{u}_n$ in Ω_b:

$$(S_l)_{ij} = \phi_j(x_i),$$

where ϕ_j is the j-th finite element basis function for $\mathbf{u}_l$. Then, we can express the functional as the sum of the squared differences between local and nonlocal solution at each point on Ω_b corresponding to a degrees of freedom

[4]Here we assume that the components of $\mathbf{u}_n$ corresponding to material points in Ω_b are the last entries of the vector.

of $\mathbf{u}_n$, i.e.

$$J_d(\mathbf{u}_n, \mathbf{u}_l) = \frac{1}{2} \sum_{i=1}^{N_b} \left((S_n \mathbf{u}_n)_i - (S_l \mathbf{u}_l)_i \right)^2 V_i, \tag{30}$$

where V_i is the volume associated with the i-th material point.

4.2. A gradient–based method for the solution of the optimization problem

We perform the optimization following the discretize–then–optimize paradigm. A general gradient–based algorithm proceeds as follows.

Given an initial guess for the discrete control variables $\boldsymbol{\theta}_n^0, \boldsymbol{\theta}_l^0$, perform the following steps, for $k = 0, 1, 2, \ldots$.

1. Solve the nonlocal and local discretized problems to obtain $\mathbf{u}_n^k$ and $\mathbf{u}_l^k$ corresponding to $\boldsymbol{\theta}_n^k, \boldsymbol{\theta}_l^k$ and evaluate the functional $J_d(\mathbf{u}_n^k, \mathbf{u}_l^k)$.
2. Compute the total derivative of the functional $J_d\left(\mathbf{u}_n(\boldsymbol{\theta}_n^k), \mathbf{u}_l(\boldsymbol{\theta}_n^k)\right)$ with respect to the control parameters at $\boldsymbol{\theta}_n^k, \boldsymbol{\theta}_l^k$. Stop if the norm of the functional derivative is smaller than a given tolerance.
3. Compute the increments $\delta(\boldsymbol{\theta}_n^k)$ and $\delta(\boldsymbol{\theta}_l^k)$ using the value of the functional and its derivative computed in steps 1 and 2.
4. Set $\boldsymbol{\theta}_n^{k+1} = \boldsymbol{\theta}_n^k + \delta(\boldsymbol{\theta}_n^k)$, and $\boldsymbol{\theta}_l^{k+1} = \boldsymbol{\theta}_l^k + \delta(\boldsymbol{\theta}_l^k)$. Go to step 1 and repeat the procedure until the desired convergence has been achieved.

The derivative of the functional in Step 2 is obtained using the adjoint based approach (see e.g. [14]). Step 3 depends on the optimization method used to solve the problem, e.g. gradient, conjugate gradient, quasi–Newton, etc. In the numerical results presented in the next section we utilize the BFGS method as implemented in the Trilinos (www.trilinos.org) [16] package *ROL*, combined with a backtrack line search.

5. Numerical tests

In this section we demonstrate the optimization–based LtN coupling strategy via two example simulations. We first present a linear patch test, followed by a simulation that includes a discontinuity in the nonlocal domain. Though preliminary, the results show the effectiveness of the coupling method and provide the basis for realistic engineering analyses.

The simulations utilize the following nonlocal kernel,

$$\gamma(\boldsymbol{x},\boldsymbol{y}) = \begin{cases} \dfrac{3}{\pi\varepsilon^4}\dfrac{1}{\|\boldsymbol{x}-\boldsymbol{y}\|} & \|\boldsymbol{x}-\boldsymbol{y}\| \le \varepsilon \\ 0 & \text{otherwise,} \end{cases} \tag{31}$$

which is often used in the literature, including in a linear peridynamic model for solid mechanics. The energy space associated with this kernel is not equivalent to a Sobolev space, but is nonetheless a separable Hilbert space whose energy norm satisfies a nonlocal Poincaré inequality.

The example simulations are carried out using the *Albany*[5][29] and *Peridigm*[6][26] codes, developed in the Center for Computing Research at Sandia National Laboratories. *Albany* is a finite–element code for simulating a variety of physical processes governed by partial differential equations. It is applied for the majority of the computation, including finite–element assembly for the local Laplacian, calculation of the functional and its derivative, and solution of the state and adjoint systems. *Peridigm* is a peridynamics code initially developed for solid mechanics and extended in this study for application to nonlocal diffusion. Specifically, *Peridigm* is employed for the solution of $(3)_1$ with the kernel given by (31). A software interface was developed to facilitate the linking of *Peridigm* routines with *Albany*, enabling the evaluation of the entirety of (13) within a single executable. Both *Albany* and *Peridigm* rely on several *Trilinos* packages, for example, *Epetra* for the management of parallel data structures, *Intrepid* for finite–element assembly, and *Ifpack* and *AztecOO* for the preconditioning and solution of linear systems. We applied the LBFGS optimization algorithm, as implemented in the *Trilinos* package *ROL*[7], in combination with a backtrack line search for solution of (14).

Linear patch test. We perform a patch test simulation to demonstrate the ability of a coupled local–nonlocal system to recover a known linear solution. The geometric configuration of the test is presented in Figure 3a. The nonlocal problem $(13)_1$ is prescribed in
$\Omega_n := [-0.8125, 0.1875] \times [-0.25, 0.25] \times [-0.125, 0.125]$,

[5]The *Albany* code can be obtained from its public github repository: https://github.com/gahansen/Albany

[6]The *Peridigm* code can be obtained at: https://peridigm.sandia.gov

[7]The *ROL* code can be obtained at: https://trilinos.org/packages/rol

and the local problem $(13)_2$ in
$\Omega_l := [-0.1875, 0.8125] \times [-0.25, 0.25] \times [-0.125, 0.125]$.
The nonlocal interaction radius ε is set to 0.125. The overlap of the local and nonlocal domains is
$\Omega_b := [-0.1875, 0.1875] \times [-0.25, 0.25] \times [-0.125, 0.125]$.
As illustrated in Figure 4, the manufactured solution $u^*_{anl} = \frac{0.001\,x}{1.625}$ is prescribed as a Dirichlet condition in the region $-0.8125 \leq x \leq -0.71875$ (for nonlocal diffusion) and on the plane $x = 0.8125$ (for local diffusion). The control Dirichlet conditions, initialized to zero, are prescribed in the nonlocal domain on $0 \leq x \leq 0.1875$ and in the local domain on the plane $x = -0.1875$. Homogeneous Neumann conditions are prescribed on the remaining portion of the domain boundary. As shown in Figures 3b and 4, the optimization–based LtN coupling approach is successful in producing the expected linear solution.

Simulation containing a discontinuity. We perform a simulation containing a discontinuity to confirm the effectiveness of the nonlocal model within a coupled local–nonlocal system. The simulation is designed such that (non–control) Dirichlet boundary conditions are applied to the local model only. This decision was motivated by the practical difficulties in applying volume constraints to nonlocal models on nontrivial configurations. Effectively, the LtN approach enables the transmission of local boundary conditions to the nonlocal model.

The configuration for the simulation containing a discontinuity is shown in Figure 5a. The nonlocal domain is defined as
$\Omega_n := [-0.9375, 0.9375] \times [-0.25, 0.25] \times [-0.125, 0.125]$.
The simulation contains two local domains, defined over the regions
$\Omega_{l1} := [-1.0625, -0.5625] \times [-0.25, 0.25] \times [-0.125, 0.125]$ and
$\Omega_{l2} := [0.5625, 1.0625] \times [-0.25, 0.25] \times [-0.125, 0.125]$.
The overlap domains are prescribed as
$\Omega_{b1} := [-0.9375, -0.5625] \times [-0.25, 0.25] \times [-0.125, 0.125]$ and
$\Omega_{b2} := [0.5625, 0.9375] \times [-0.25, 0.25] \times [-0.125, 0.125]$,
and the nonlocal interaction radius as $\varepsilon = 0.125$. The control Dirichlet conditions, again initialized to zero, are prescribed in the nonlocal domain on $-0.9375 \leq x \leq -0.5625$ and $0.5625 \leq x \leq 0.9375$, and in the local domain on the planes $x = -1.0625$ and $x = 1.0625$. A discontinuity is inserted into the model via a rectangular plane defined by $x = 0$, $0 \leq y \leq 0.25$, and $-0.125 \leq z \leq 0.125$. Here, the visibility between material points separated

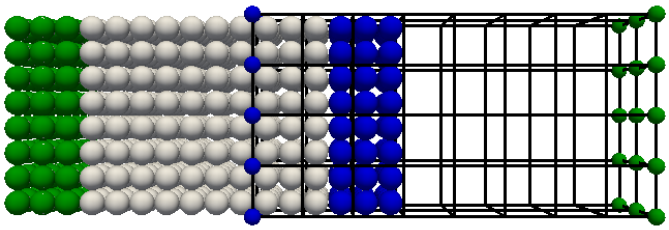

(a) Configuration for the patch test simulation. Dirichlet boundary conditions are applied to the nodes highlighted in green. Control nodes are highlighted in blue.

(b) Solution u for the patch test simulation.

Figure 3: Linear patch test simulation.

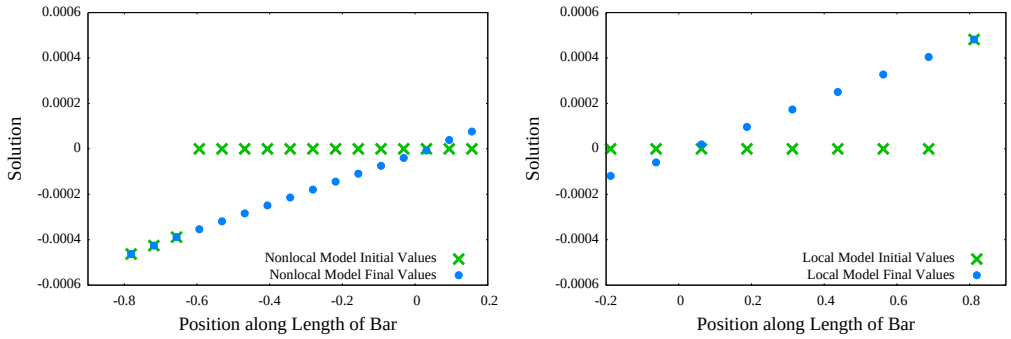

(a) Nonlocal model. (b) Local model.

Figure 4: Initial and final values for the patch test for a set of points aligned with the horizontal axis.

by the plane is disallowed.

Simulation results are presented in Figures 5b and 6. In Figure 5b, the discontinuity appears as a jump in the solution at $x = 0$ that runs vertically from the top of the bar to the center of the bar. The ability of the nonlocal model to capture the discontinuous solution is better illustrated in Figure 6. The discontinuous solution along the top of the bar is shown in Figure 6b, and the continuous solution along the bottom of the bar in Figure 6d.

The example simulations demonstrate the utility and effectiveness of optimization–based LtN coupling for the recovery of a known linear solution, the application of local boundary conditions to a coupled local–nonlocal system, and the modeling of a discontinuity within the nonlocal domain. These preliminary results serve as the groundwork for the ongoing development of engineering analysis tools.

Acknowledgments

This material is based upon work supported by the US DOE's Laboratory Directed Research and Development (LDRD) program at Sandia National Laboratories and the U.S. Department of Energy, Office of Science, Office of Advanced Scientific Computing Research. Part of this research was carried under the auspices of the Collaboratory on Mathematics for Mesoscopic Modeling of Materials (CM4).

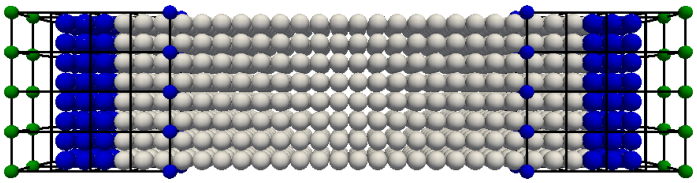

(a) Configuration for the example simulation with a discontinuity in the nonlocal domain. Dirichlet boundary conditions are applied to the nodes highlighted in green, which reside in the local domain. Control nodes are highlighted in blue.

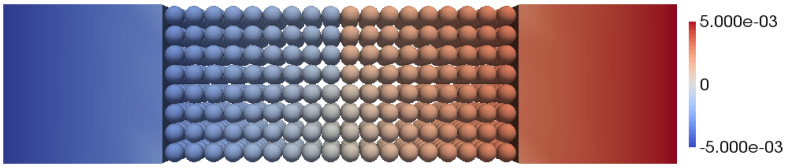

(b) Solution u for the example simulation with a discontinuity in the nonlocal domain. A discontinuity is present in the center of the bar, resulting in a jump in the solution u along the top edge of the bar.

Figure 5: Simulation of a bar containing a discontinuity. The discontinuity extends vertically from the top of the bar halfway through the height of the bar. Dirichlet boundary conditions are applied to the ends of the bar (local domain), circumventing the need to prescribe volume constraints in the nonlocal domain.

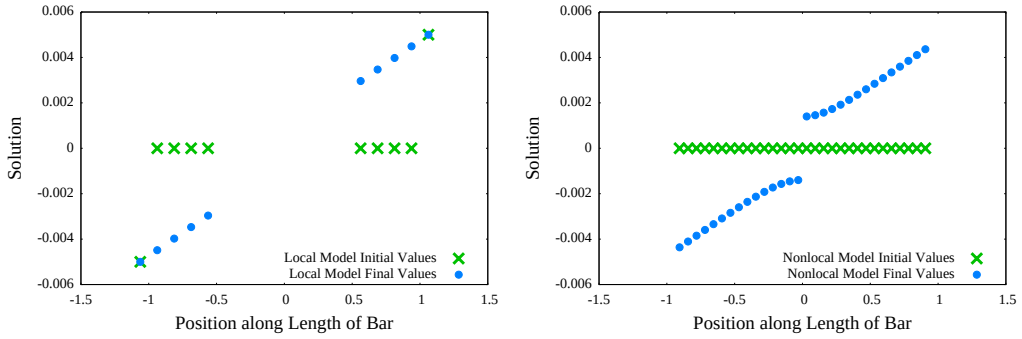

(a) Local model, top of bar.

(b) Nonlocal model, top of bar.

(c) Local model, bottom of bar.

(d) Nonlocal model, bottom of bar.

Figure 6: Initial and final values for the simulation containing a discontinuity for a set of points aligned with the horizontal axis. Solution values are plotted for points along the top of the bar, which contains a discontinuity, and also for points along the bottom of the bar, which does not contain a discontinuity.

References

[1] B Aksoylu and M Parks. Towards domain decomposition for nonlocal problems. Technical Report arXiv:0909.4504, 2009.

[2] Yan Azdoud, Fei Han, and Gilles Lubineau. A morphing framework to couple non-local and local anisotropic continua. *International Journal of Solids and Structures*, 50(9):1332 – 1341, 2013.

[3] S. Badia, P. Bochev, M. Gunzburger, R. Lehoucq, and M. Parks. Blending methods for coupling atomistic and continuum models. In J. Fish, editor, *Bridging the scales in science and engineering*, pages 165–186. Oxford University Press, 2009.

[4] Jaydeep P. Bardhan. "gradient models in molecular biophysics: Progress, challenges, opportunities.". *Journal of the mechanical behavior of materials*, 22.5-6:169–184, 2013.

[5] N. Burch and R.B. Lehoucq. Classical, nonlocal, and fractional diffusion equations on bounded domains. *International Journal for Multiscale Computational Engineering*, 9:661–674, 2011.

[6] X. Chen and Max Gunzburger. Continuous and discontinuous finite element methods for a peridynamics model of mechanics. *Computer Methods in Applied Mechanics and Engineering*, 200(9–12):1237 – 1250, 2011.

[7] M. D'Elia and P. Bochev. Formulation, analysis and computation of an optimization–based local–to–nonlocal coupling method. Sandia Report SAND, Sandia National Laboratories, Sandia National Laboratories Albuquerque, New Mexico 87185, 2015.

[8] M. D'Elia and P. Bochev. Optimization–based coupling of nonlocal and local diffusion models. In *2014 MRS Fall Meeting Proceedings*, 2015.

[9] M. D'Elia, Q. Du, M. D. Gunzburger, and R. B. Lehoucq. Finite range jump processes and volume–constrained diffusion problems. Technical Report SAND2014–2584J, Sandia National Laboratories, 2014.

[10] Hashmi Ben Dhia and Guillaume Rateau. The Arlequin method as a flexible engineering design tool. *International Journal for Numerical Methods in Engineering*, 62(11):1442–1462, 2005.

[11] M. Di Paola, G. Failla, and M. Zingales. Physically-based approach to the mechanics of strong non-local linear elasticity theory. *Journal of Elasticity*, 97(2):103–130, 2009.

[12] Q. Du, M. Gunzburger, R. Lehoucq, and K. Zhou. Analysis and approximation of nonlocal diffusion problems with volume constraints. *SIAM Review*, 54(4):667–696, 2012.

[13] Q. Du, M. Gunzburger, R. B. Lehoucq, and K. Zhou. A nonlocal vector calculus, nonlocal volume–constrained problems, and nonlocal balance laws. *Mathematical Models and Methods in Applied Sciences*, 23(03):493–540, 2013.

[14] M. D. Gunzburger. *Perspectives in Flow Control and Optimization*. Society for Industrial and Applied Mathematics, Philadelphia, PA, USA, 2002.

[15] Fei Han and Gilles Lubineau. Coupling of nonlocal and local continuum models by the Arlequin approach. *International Journal for Numerical Methods in Engineering*, 89(6):671–685, 2012.

[16] M. A. Heroux, R. A. Bartlett, V. E. Howle, R. J. Hoekstra, J. J. Hu, T. G. Kolda, R. B. Lehoucq, K. R. Long, R. P. Pawlowski, E. T. Phipps, A. G. Salinger, H. K. Thornquist, R. S. Tuminaro, J. M. Willenbring, A. Williams, and K. S. Stanley. An overview of the Trilinos project. *ACM Trans. Math. Softw.*, 31(3):397–423, 2005.

[17] A. Hildebrandt, R. Blossey, S. Rjasanow, O. Kohlbacher, and H.-P. Lenhof. Novel formulation of nonlocal electrostatics. *Phys. Rev. Lett.*, 93:108104, Sep 2004.

[18] k. Zhou and Q. Du. Mathematical and numerical analysis of linear peridynamic models with nonlocal boundary conditions. *SIAM J. Numer. Anal.*, 48(5):1759–1780, 2010.

[19] D.J. Littlewood. Roadmap for peridynamic software implementation. SAND Report, Sandia National Laboratories, Albuquerque, NM and Livermore, CA, 2015.

[20] Gilles Lubineau, Yan Azdoud, Fei Han, Christian Rey, and Abe Askari. A morphing strategy to couple non-local to local continuum mechanics. *Journal of the Mechanics and Physics of Solids*, 60(6):1088 – 1102, 2012.

[21] M. Luskin and C. Ortner. Atomistic-to-continuum coupling. *Acta Numerica*, 22:397–508, 4 2013.

[22] R. Miller and E. Tadmor. A unified framework and performance benchmark of fourteen multiscale atomistic/continuum coupling methods. *Modeling and Simulation in Materials Science and Engineering*, 17(5):053001, 2009.

[23] D. Olson, P. Bochev, M. Luskin, and A. Shapeev. An optimization-based atomistic-to-continuum coupling method. *SIAM Journal on Numerical Analysis*, 52(4):2183–2204, 2014.

[24] D. Olson, A. Shapeev, P. Bochev, and M. Luskin. Analysis of an optimization-based atomistic-to-continuum coupling method for point defects. *Mathematical Modeling and Numerical Analysis (ESAIM)*, Accepted, 2015.

[25] M.D. Gunzburger P. Seleson, M.L. Parks and R.B. Lehoucq. Peridynamics as an upscaling of molecular dynamics. *Multiscale Modeling and Simulation*, 8:204–227, 2009.

[26] M. L. Parks, D. J. Littlewood, J. A. Mitchell, and S. A. Silling. Peridigm Users' Guide v1.0.0. SAND Report 2012-7800, Sandia National Laboratories, Albuquerque, NM and Livermore, CA, 2012.

[27] R. Phillips. *Crystals, defects and microstructures: modeling across scales*. Cambridge University Press, 2001.

[28] L. Tian Q. Du, L. Ju and K. Zhou. A posteriori error analysis of finite element method for linear nonlocal diffusion and peridynamic models. *Mathematics of computation*, 82:1889–1922, 2013.

[29] A.G. Salinger, R.A. Bartlett, Q. Chen, X. Gao, G.A. Hansen, I. Kalashnikova, A. Mota, R.P. Muller, E. Nielsen, J.T. Ostien, R.P. Pawlowski, E.T. Phipps, and W. Sun. Albany: A component–based partial differential equation code built on trilinos. SAND Report 2013-8430J, Sandia National Laboratories, Albuquerque, NM and Livermore, CA, 2013.

[30] Sandro Salsa. *Partial Differential Equations in Action : From Modelling to Theory*. Universitext. Springer-Verlag Italia Milano, Milano, 2008.

[31] Pablo Seleson, Samir Beneddine, and Serge Prudhomme. A force-based coupling scheme for peridynamics and classical elasticity. *Computational Materials Science*, 66(0):34 – 49, 2013. Multiscale simulation of heterogeneous materials and coupling of thermodynamic models.

[32] S. A. Silling. Reformulation of elasticity theory for discontinuities and long-range forces. *Journal of the Mechanics and Physics of Solids*, 48(1):175 – 209, 2000.

[33] S. A. Silling and E. Askari. A meshfree method based on the peridynamic model of solid mechanics. *Computers and Structures*, 83:1526–1535, 2005.

[34] S.A. Silling and R.B. Lehoucq. In Hassan Aref and Erik van der Giessen, editors, *Peridynamic Theory of Solid Mechanics*, volume 44 of *Advances in Applied Mechanics*, pages 73 – 168. Elsevier, 2010.

[35] E. B. Tadmor, M. Ortiz, and R. Phillips. Quasicontinuum analysis of defects in solids. *Philosophical Magazine A*, 73(6):1529–1563, 1996.